Available online at www.sciencedirect.com
SCIENCE DIRECT®
Journal of Power Sources 124 (2003) 278–284
JOURNAL OF POWER SOURCES
www.elsevier.com/locate/jpowsour

Studies on the oxygen reduction catalyst for zinc–air battery electrode

Xianyou Wang [a,c,*], P.J. Sebastian [a,b], Mascha A. Smit [a], Hongping Yang [c], S.A. Gamboa [b]

[a] *Centro de Investigación en Energía-UNAM, 62580 Temixco, Morelos, Mexico*
[b] *IMP, Programa de Investigación y Desarrollo de Ductos, Eje Central Lázaro, Cárdenas 152, 07730, D.F., Mexico*
[c] *College of Chemistry, Xiangtan University, Hunan 411105, China*

Received 24 April 2003; accepted 19 May 2003

Abstract

In this paper, perovskite type $La_{0.6}Ca_{0.4}CoO_3$ as a catalyst of oxygen reduction was prepared, and the structure and performance of the catalysts was examined by means of IR, X-ray diffraction (XRD), and thermogravimetric (TG). Mixed catalysts doped, some metal oxides were put also used. The cathodic polarization curves for oxygen reduction on various catalytic electrodes were measured by linear sweep voltammetry (LSV). A Zn–air battery was made with various catalysts for oxygen reduction, and the performance of the battery was measured with a BS-9300SM rechargeable battery charge/discharge device. The results showed that the perovskite type catalyst ($La_{0.6}Ca_{0.4}CoO_3$) doped with metal oxide is an excellent catalyst for the zinc–air battery, and can effectively stimulate the reduction of oxygen and improve the properties of zinc–air batteries, such as discharge capacity, etc.

Keywords: Perovskite catalyst; Air-electrode

1. Introduction

The great efforts are made worldwide to develop battery systems having high specific energy. The demand for such systems has risen dramatically in recent times, particularly in connection with electric traction, the storage of electrical energy from photovoltaic installations and the operation of portable devices. Among all batteries, because of its steady performance, source of raw material and low-cost, the study and development the of zinc–air battery is paid more and more attention. Because of their high specific energy ($100\,Wh\,kg^{-1}$) and inexpensive and environmentally benign materials, Zn–air batteries are promising energy storage devices [1].

It is a special feature of the zinc–air system that only the active component of the negative electrode (zinc) needs to be stored in the battery, while the reactant for the positive electrode (oxygen) during discharge is drawn from the air. This is the basis for the system's high specific energy—distinctly higher than that of conventional battery systems (Lead–acid, Ni/Cd, Ni/MH).

There are two kinds of Zn–air batteries, primary and rechargeable. The key problem the development of Zn–air batteries is the oxygen-diffusion electrode. Usually, it is a porous, carbon-based oxygen-diffusion electrode consisting of a mixture of catalysts and carbon. Various types of electrocatalysts, e.g. Pt and Pt–Ru alloys have been investigated as a key component of the electrodes, but they are expensive. Significant progress has been made in recent years in the development of less expensive electrocatalysts such as perovskite (e.g. $La_{1-x}Ca_xCoO_3$), spinels (e.g. Co_3O_4, $NiCo_2O_4$), pyrochlores (e.g. $Pb_2Ru_2Pb_{1-x}O_{1-y}$, $Pb_2Ru_2O_{6.5}$), other oxides (e.g. $Na_{0.8}Pt_3O_4$), and pyrolyzed macrocycles with Co additives [2].

Due to the cost of the catalyst, non-noble catalysts such as metal oxides in the form of perovskites, pyrochlores, and spinels are preferred over noble metals for activating the air electrode for the oxygen reduction and evolution reactions [3–5]. The perovskite catalyst ($La_{0.6}Ca_{0.4}CoO_3$) was widely studied as a cathode material for Zn–air batteries, owing to its high catalytic activity for oxygen reduction. The active layer contains perovskite catalyst ($La_{0.6}Ca_{0.4}CoO_3$) [3] supported by graphitized carbon and bonded with PTFE. The gas-diffusion layer consists of PTFE-bonded carbon black.

The perovskite-type catalysts have been investigated for improvement in the preparation method, promotion effects by partially substituting A or B cations, and adsorption phenomenon of oxygen the characterization of the surface properties, etc. [6]. Sr-substitution (0.1–0.4 mol) for La in the $LaCoO_3$ lattice has been observed to improve both the

* Corresponding author. Fax: +52-777-325-0018.
E-mail address: wxianyou@yahoo.com (X. Wang).

0378-7753/$ – see front matter © 2003 Elsevier B.V. All rights reserved.
doi:10.1016/S0378-7753(03)00737-7

real surface area as well as the apparent catalytic activity of the oxide towards O_2 evolution in alkaline solution; the enhancement in surface area was found to be 2–5-fold [5,8].

Recently, Tiwari et al. [5] synthesized $La_{1-x}Sr_xCoO_3$ ($0 \leq x \leq 0.5$) and $La_{0.8}Sr_{0.2}Co_{1-y}B_yO_3$ (B = Ni; Fe; Cu or Cr; $0 \leq y \leq 0.3$) using malic acid and observed that the $LaCoO_3$ electrode with $x = 0.2$ was the most active and that 0.1 mol Fe/or Ni substitution at the B site further improved considerably both the apparent (i_a) and true activity (i_t) towards electrolytic evolution of O_2 in 1 M KOH at 25 °C.

Although the perovskite catalyst $La_{0.6}Ca_{0.4}CoO_3$ has been studied in detail, we consider that it is improved by using mixed catalysts with other metal oxides. In this paper, in order to obtain a relatively more efficient oxygen electrode by a simpler and low-cost method, we report a method for perovskite catalyst ($La_{0.6}Ca_{0.4}CoO_3$) using co-precipitation and calcining, and have investigated the physicochemical and electrocatalytic properties towards O_2 reduction reaction, especially with the performance of the perovskite catalyst doped metal oxides.

2. Experimental

2.1. Sample preparation

The catalyst $La_{0.6}Ca_{0.4}CoO_3$ powder was prepared by an amorphous citrate precursor method [9]. A solution containing a mixture of citric acid and constituent metal nitrates, including $La(NO_3)_3$, $Ca(NO_3)_2$, and $Co(NO_3)_2$, was gradually evaporated at 75 °C until a blue paste was formed. The molar ratio of citric acid to the metal nitrates was 1:1, and the molar ratio of metal nitrates for $La(NO_3)_3$, $Ca(NO_3)_2$, and $Co(NO_3)_2$ is 0.6:0.4:0.1. The blue paste continued to dry at 90 °C for 48 h until it changed into a blue solid; the solid was then pre-calcined at 200 °C for 2.5 h and continued to calcine for 2.5 h at increasing temperatures up to 700 °C to form the perovskite phase. The resulted powder was then further annealed in vacuum (500–600 °C; B 0.01 Torr) for 1 h to create oxygen deficiencies.

2.2. Sample characterization

The powder X-ray powder diffraction patterns of the substituted spinels were obtained using the X-ray diffraction (XRD) method employing Cu Kα radiation (Rigaku, Miniflex Co. Ltd.).

Thermogravimetric (TG)/derivative thermogravimetric (DTG) measurements were carried out by using a Rigaku PTC-10A thermal analyzer with a nitrogen flow of 70 ml min^{-1} at a rate of 10 °C min^{-1} from room temperature to 800 °C. About 10 mg of sample was used in each test.

IR spectra were attained at room temperature with the help of a Nicolet 510P FT-IR spectrometer.

2.3. Electrode preparation and electrochemical measurement

The mixed catalyst doped some metal oxides was consist of $La_{0.6}Ca_{0.4}CoO_3$ and metal oxides. To prepare the active layer of the air electrode, a mixture containing $La_{0.6}Ca_{0.4}CoO_3$, metal oxides, and carbon black was ball-milled in the ball-milled machine for 0.5 h, then the mixture and PTFE suspension (60 wt.% in H_2O) with weight ratios of 9:1 were first mixed and ground in excess ethanol and then dried at 85 °C to give a dough-like paste, which was finally rolled into a thin layer of 200 μm thickness. A diffusion layer containing only carbon black and PTFE was prepared by the same process.

The air electrode was characterized with a three-electrode configuration with a nickel foam counter-electrode and a Hg/HgO/OH^- (7 M) reference electrode. The electrolyte is 7 M KOH, purified by electrolysis under nitrogen atmosphere and maintained at 25 °C. The polarization curves were acquired on an electrochemical work station (CHI 660A) under a constant potential-sweep rate of 5 mV s^{-1}.

The air-electrodes are composed of two layers. A hydrophobic gas diffusion layer (on the gas side) containing carbon black and PTFE and an active layer (on the electrolyte side), containing the $La_{0.6}Ca_{0.4}CoO_3$ perovskite catalyst supported on graphite like carbon material and PTFE. The carbon material was Vulcan XC72 (Cabot). Both layers, together with a nickel foam current collector on top of the gas diffusion layer, were pressed together at 40 MPa for 5 min. The thicknesses of the electrodes used in the experiment were typically 0.6 mm.

The cell-discharge capacity was measured and compared with the commercial alkaline Zn–MnO_2 battery by BS-9300SM rechargeable battery charge/discharge device. The discharge current is 10 mA and the cut-off voltage is 0.8 V.

3. Results and discussion

3.1. Examination and analysis of structure

Powder X-ray diffraction results indicated that the materials were single-phase cubic perovskite structures or distorted cubic structures. Fig. 1 is the XRD pattern for perovskite catalyst $La_{0.6}Ca_{0.4}CoO_3$. XRD analysis (Fig. 1) and showed that the reflection from the powder were not consistent with a single-phase $La_{0.6}Ca_{0.4}CoO_3$ [10]. The peaks are sharper and more intense, suggesting better crystallinity and larger crystallites. No detectable position shifts of the diffraction lines were observed. However the powder retained about the same lattice structure, there was the appearance of Co_3O_4 and La_2O_3 phases (Co_3O_4 ($d = 2.44$), $La(OH)_3$ ($d = 2.91$, 3.526)) as well as shrinkage in unit-cell parameters.

The thermogravimetric (mass loss, TG) and derivative thermogravimetric (rate of mass loss, DTG) curves of 5 mg

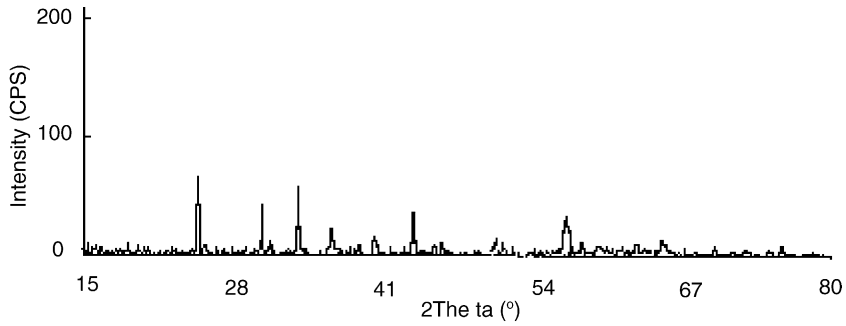

Fig. 1. XRD pattern of the catalyst $La_{0.6}Ca_{0.4}CoO_3$.

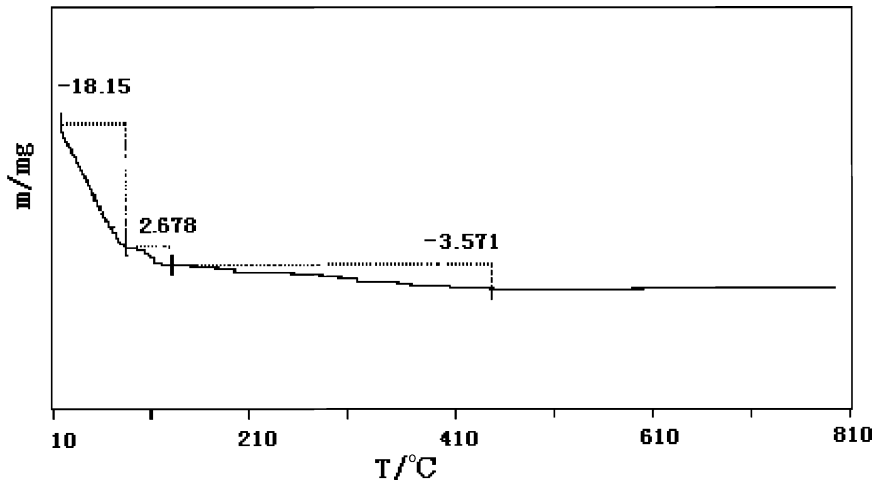

Fig. 2. TG analysis of the catalyst $La_{0.6}Ca_{0.4}CoO_3$.

of $La_{0.6}Ca_{0.4}CoO_3$ are given in Figs. 2 and 3, respectively. When the curves are compared, four different regions can be distinguished as follows: from ambient to 128 °C, between 128 and 200 °C, from 200 to 280 °C, from 280 to 300 °C. By 300 °C the formation of the solid oxide corresponding to a total mass loss of approximately 25.345% is complete. It can be seen from Fig. 1 that the thermogravimetric curve abruptly decreases from ambient to 128 °C, and it can be seen from Fig. 2 that the thermogravimetric curve has a strong peak at 102.9 °C. This peak has a mass loss of approximately 21.828% and represents water loss in perovskite catalyst $La_{0.6}Ca_{0.4}$ CoO_3. From 200 to 280 °C, another strong peak appears at 152.4 °C. This peak may represent further oxidation of some elements, e.g. Co compound was oxidized into Co_3O_4 and La_2O_3 was formed, which has been found from X-ray diffraction results (in Fig. 1). At

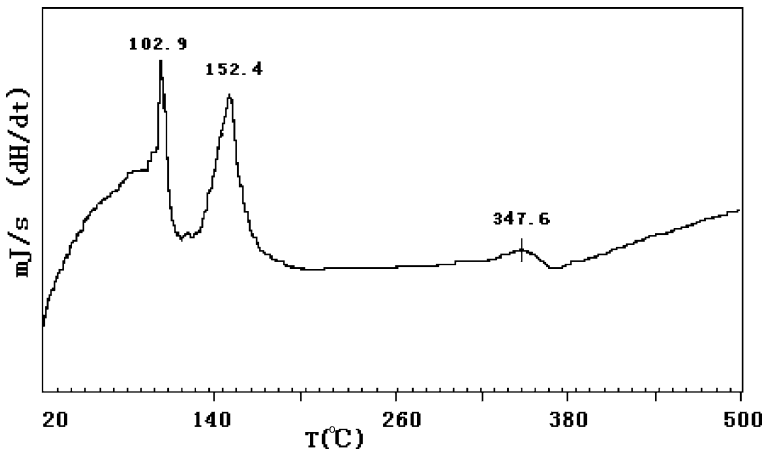

Fig. 3. DTG analysis of the catalyst $La_{0.6}Ca_{0.4}CoO_3$.

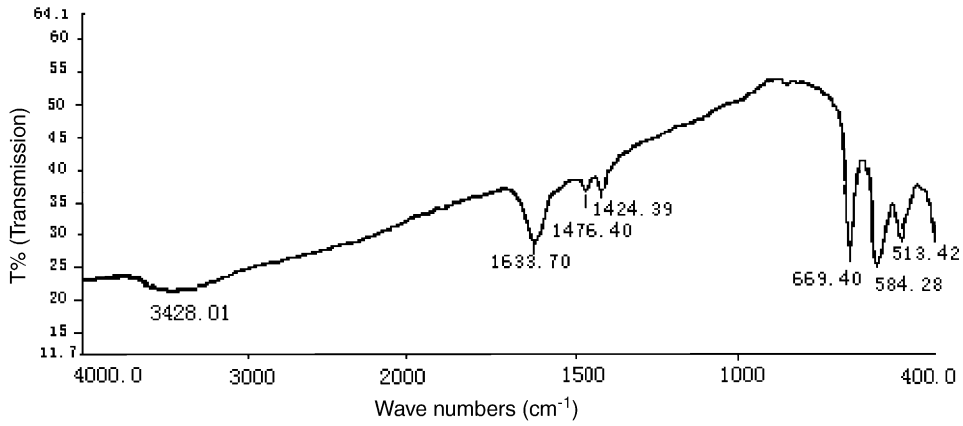

Fig. 4. FAR-IR spectrum of the catalyst $La_{0.6}Ca_{0.4}CoO_3$.

347.6 °C, a weak peak can be found. Usually, this peak is considered to be due to phase change. By 300 °C, a stable perovskite compound has formed.

Fig. 4 presents the FTIR spectra of the perovskite catalyst $La_{0.6}Ca_{0.4}$ CoO_3. IR spectra of oxide in the region of 4000–400 cm^{-1} exhibited some bands, the strong bands at 600–700 and 540–600 cm^{-1}, and a weak band at 420–520 cm^{-1} (Fig. 4). The strong band is characteristic of a pure perovskite phase and can be ascribed to the (Co–O) vibration [11,12]. The broad and centered at 3428 cm^{-1} is due to the ν_{O-H} vibration of H-bonded water molecules located in the interlamellar space of the perovskite catalyst $La_{0.6}Ca_{0.4}CoO_3$.

3.2. Polarization curves measurement

The Zn–air battery has a theoretical battery voltage 1.65 V. The overall battery discharge reactions can be summarized as follows [13].

At the positive electrode:

$$O_2 + 2H_2O + 4e \rightarrow 4OH^-; \quad E^0 = 0.40\,V \tag{1}$$

At the negative electrode:

$$2Zn \rightarrow 2Zn^{2+} + 4e \tag{2}$$

$$2Zn^{2+} + 4OH^- \rightarrow 2Zn(OH)_2; \quad E^0 = 1.25\,V \tag{3}$$

$$2Zn(OH)_2 \rightarrow 2ZnO + 2H_2O \tag{4}$$

Overall battery reaction:

$$2Zn + O_2 \rightarrow 2ZnO; \quad E^0 = 1.65\,V \tag{5}$$

As seen from above reactions (1)–(5), the key electrode reaction for Zn–air battery is the oxygen reduction reaction. The oxygen reduction process is complex and involves a rate-limiting step which affects the reaction kinetics and the battery performance. This stage involves the formation of hydroperoxide ions HO_2^-, catalysts are required to accelerate the decomposition of these hydroperoxide ions.

Usually, for the two reactions occurring at the O_2 electrode (see reactions (6)–(7)), is adopted the mechanism proposed in [10], where the reduction of O_2 to OH^- in alkaline solution occurs via an intermediate peroxide HO_2^-. The first step, O_2 reduction to HO_2^- (reaction (6)), is considered to follow the reaction equation:

$$O_2 + H_2O + 2e \rightarrow HO_2^- + OH^- \tag{6}$$

The intermediate HO_2^- then reacts by catalytic disproportionation to O_2 and OH^- (reaction (7)):

$$HO_2^- \rightarrow \tfrac{1}{2}O_2 + OH^- \tag{7}$$

Therefore, in order to study the effect of the catalyst on the oxygen reduction reaction, Fig. 5 shows the cathode polarization curves of electrodes with different catalyst amounts. The curve which has 5 wt.% catalyst showed the highest current. The others showed lower current, but were very similar in current magnitude and Tafel slope (see Fig. 6). To compare the characteristics of the electrodes, the results of the

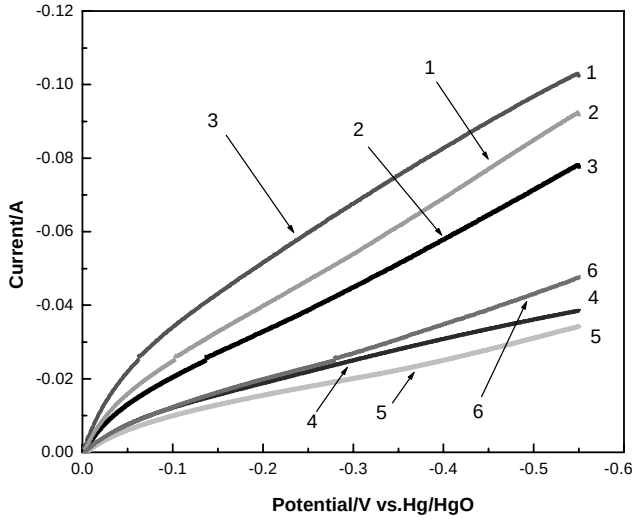

Fig. 5. Cathodic polarization curves of electrodes with different catalyst amount. Catalyst $La_{0.6}Ca_{0.4}CoO_3$ content: (1) 5%; (2) 10%; (3) 15%; (4) 20%; (5) 25%; (6) 30%.

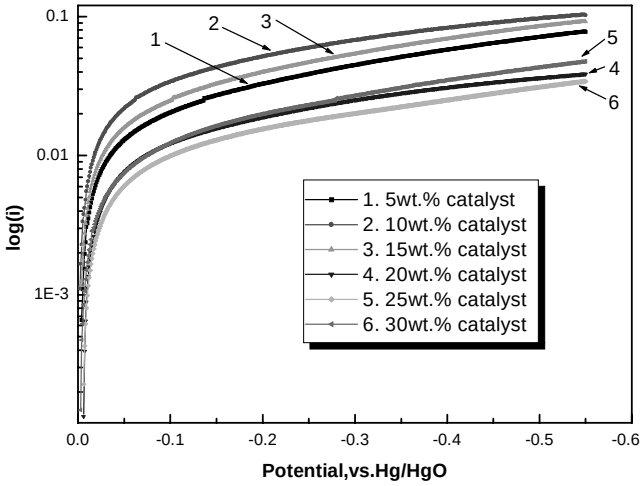

Fig. 6. Tafel plots of *I–V* data in Fig. 5.

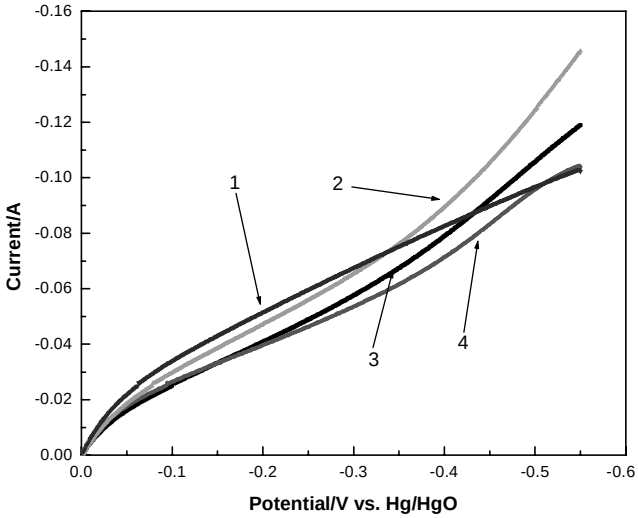

Fig. 7. Cathodic polarization curves of different catalytic electrodes doped different compounds. Catalyst: (1) $La_{0.6}Ca_{0.4}CoO_3$ 15%, (2) $La_{0.6}Ca_{0.4}CoO_3$ 15%, MnO_2 5% and $Ni(OH)_2$ 15%, (3) $La_{0.6}Ca_{0.4}CoO_3$ 15% and MnO_2 20%, (4) $La_{0.6}Ca_{0.4}CoO_3$ 15%, MnO_2 15% and CaO 5%.

polarization study in Fig. 5 are tabulated in Table 1 where the currents at fixed potentials are tabulated and the value of $\Delta I/\Delta\Phi$ is given for each curve in Fig. 5, this value came from the data in Fig. 5 at a potential −0.2 and −0.5 V and can be used to determine the effects of the catalyst on polarization of the oxygen reduction reaction. From Table 1, the curve which has 15 wt.% catalyst displayed the highest value and this indicates that this curve has smallest polarization for the oxygen reduction reaction.

Shown in Fig. 6 are the Tafel plots of the data in Fig. 5. As expected, the data showed very flat Tafel regions. At any given potential, the electrodes with different catalyst contents gave different polarization behavior and suggest different electrocatalytic activity.

In Fig. 6 the reduction of oxygen has two Tafel zones. Rios et al. [14] studied the correlations between electrocatalytic activities towards reduction of oxygen on powder electrodes of cobalt and manganese spinel type oxides $Mn_xCo_{3-x}O_4$ and found that the Tafel curve was also divided into two regions. Wu et al. [7] found that catalytic activities of $La_{0.6}Ca_{0.4}CoO_{3-x}$ towards oxygen reduction and evolution were affected by two mechanisms. Thus, the mechanism of oxygen reduction reaction on the perovskite catalyst synthesized in simple method is in agreement with Wu et al. [7] and Rios et al. [14].

3.3. The mixed catalyst doped with metal oxides

Even the best catalysts that are presently available, such as Pt, show substantial irreversibility with the result that considerable energy is wasted. An improved catalyst for O_2 reduction and generation will bring improvements in the performance of fuel cells, metal–air batteries, industrial electrolytic processes, and electrochemical sensors. Despite extensive research on the O_2 electrode reaction, there is no satisfactory catalyst available that will perform in a bifunctional manner with low overpotential at practical current densities. Even with the most active catalyst, such as highly dispersed platinum, the activation overpotential for the reduction process is typically −0.3 to −0.45 V at practical current densities [15]. Wei et al [16]. reported that a catalyst prepared from carbon black mixed with pyrolytic MnO_2 was used as an air-electrode and showed a better results.

Fig. 7 shows cathode polarization curves for electrodes of mixed catalyst and graphite. The mixed catalyst was composed of perovskite $La_{0.6}Ca_{0.4}CoO_3$ and metal oxide, e.g. $Ni(OH)_2$, MnO_2, CaO. As seen from Fig. 7, the curves displayed different slopes with different catalysts. The currents and the value of $\Delta I/\Delta\Phi$ in Fig. 7 are summarized in Table 2.

Table 1
Performance comparison of different electrodes

Amount of catalyst (%)	Current at –0.2 V (A)	Current at −0.5 V (A)	$\Delta I/\Delta\Phi$
5	−0.03982	−0.06909	0.09757
10	−0.03289	−0.05786	0.083233
15	−0.05151	−0.08256	0.1035
20	−0.01890	−0.03096	0.0402
25	−0.01553	−0.02506	0.03177
30	−0.01992	−0.03490	0.04993

Table 2
Performance comparison of different catalytic electrodes doped compound

The composition of catalyst	Current at −0.1V (A)	Current at −0.3V (A)	$\Delta I/\Delta\Phi$
$La_{0.6}Ca_{0.4}CoO_3$ 15%	−0.03395	−0.06754	0.1680
$La_{0.6}Ca_{0.4}CoO_3$ 15%, MnO_2 15%, CaO 5%	−0.02971	−0.06541	0.1785
$La_{0.6}Ca_{0.4}CoO_3$ 15%, MnO_2 20%	−0.02505	−0.05788	0.1642
$La_{0.6}Ca_{0.4}CoO_3$ 15%, MnO_2 5%, $Ni(OH)_2$ 15%	−0.02640	−0.05345	0.1353

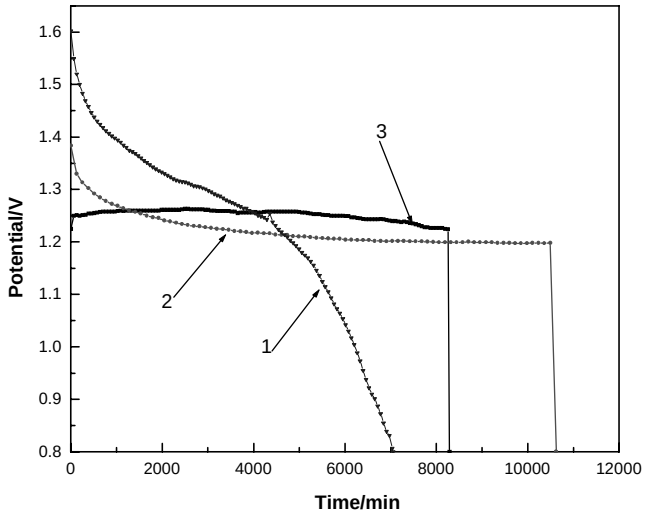

Fig. 8. Comparison of discharge curves for Zn–air battery and Nanfu alkaline Zn–MnO_2 battery. (1) Commercial Zn–MnO_2 alkaline battery, (2) Zn–air battery with the catalyst composition of $La_{0.6}Ca_{0.4}CoO_3$ 15%, MnO_2 5% and $Ni(OH)_2$ 15%, (3) Zn–air battery with $La_{0.6}Ca_{0.4}CoO_3$ 15%.

It can be found from Table 2 and Fig. 7 that curves 1 and 2 showed the larger slope, for example. This suggests that they have a lower polarization for oxygen reduction than others. However, curve 2 has much higher value of $\Delta I/\Delta \Phi$ than curve 1. This indicates that curve 2 has less polarization for the oxygen electrode reaction. Thus, mixed catalysts doped with some metal oxides have much better electrocatalytic activity for the oxygen reduction reaction.

3.4. Performance of Zn–air battery

Discharge profiles at constant current of 10 mA for Zn–air batteries with different amounts of catalysts are given in Fig. 8. It can be seen from Fig. 8 that the Zn–air batteries containing 15 wt.% $La_{0.6}Ca_{0.4}CoO_3$ 15% and $La_{0.6}Ca_{0.4}CoO_3$, MnO_2 5%, $Ni(OH)_2$ 15% as the catalyst for the air-electrode have clearly much higher discharge capacities than commercial Zn–MnO_2 alkaline batteries of the same size. Furthermore, the Zn–air battery containing $La_{0.6}Ca_{0.4}CoO_3$, MnO_2 5%, $Ni(OH)_2$ 15% as the catalyst for the air-electrode has the highest discharge capacity. For the sake of clarity, the data of curve 2 in Fig. 8 and the commercial Zn–MnO_2 alkaline battery (curve 1) are tabulated in Table 3. It can be seen from Table 3 that the discharge plateau voltage of the Zn–air battery is 1.273 V while commercial Zn–MnO_2 alkaline battery is 1.202 V.

The Zn–air battery is able to sustain the current drains, as demonstrated by the flat discharge curves (in Fig. 8). The total capacity of the Zn–air battery is limited by the Zn electrode. The air electrode itself is not discharged; it only reduces oxygen in the electrode reaction an discharge. This is the apparent difference between the Zn–air battery and the commercial Zn–MnO_2 alkaline battery. In the commercial Zn–MnO_2 alkaline battery, the capacity of the battery not only depends on the amount of Zn powder in the anode, but also on the amount of MnO_2 in the cathode. However, in the Zn–air battery, the capacity of the battery only depends on the amount of Zn powder if there is a good catalyst to sustain the reduction reaction of oxygen. The amount of catalyst in a Zn–air battery is markedly less than the amount of the cathode active material in the commercial Zn–MnO_2 alkaline battery, thus for the same size battery, the Zn–air battery has a much higher discharge capacity than the commercial Zn–MnO_2 alkaline battery. So, it can be found from Table 3 that the discharge time of the Zn–air battery lasted for 10,496 min, while the same size commercial Zn–MnO_2 alkaline battery only sustained 7055 min, that is, the capacity of the Zn–air battery is over 30% more than commercial Zn–MnO_2 alkaline battery.

Table 3
Comparison of discharge curves for Zn–air battery and Commercial alkaline Zn–MnO_2 battery

Parameters	Commercial alkaline Zn–MnO_2 battery	Zn–air battery
Discharge current (mA)	10	10
Opening circuit voltage (V)	1.602	1.383
Cut-off voltage (V)	0.8	0.8
Discharge middle voltage (V)	1.273	1.202
Initial resistance (mΩ)	4531.2	4532.8
Average resistance (mΩ)	4078.08	3885.26
Discharge time (min)	7055	10496
Discharge capacity (mAh)	1205	1819

4. Conclusion

The catalyst $La_{0.6}Ca_{0.4}CoO_3$ was synthesized under simple conditions. XRD analysis reveal that the $La_{0.6}Ca_{0.4}CoO_3$ has a perovskite structure. Electrochemical investigation showed that the perovskite catalyst $La_{0.6}Ca_{0.4}CoO_3$ is a promising electrocatalyst for oxygen reduction in alkaline media, especially as a mixed catalyst doped with other metal oxides. The data on the discharge capacity of a Zn–air battery and the same size commercial Zn–MnO_2 alkaline battery showed that the Zn–air battery has a much higher discharge capacity than the commercial Zn–MnO_2 alkaline battery.

Although the perovskite catalyst $La_{0.6}Ca_{0.4}CoO_3$ is an excellent electrocatalyst for the oxygen reduction reaction, the investigation found that a mixed catalyst, which consisted of a perovskite catalyst $La_{0.6}Ca_{0.4}CoO_3$ and some other metal oxide, represents a much better choice. This suggests that using a mixed catalyst is a much better method of manufacture of the air-electrode for metal–air battery.

Acknowledgements

The authors acknowledge the support received through the project IN102100 (DGAPA-UNAM) for this work.

References

[1] E. Deiss, F. Holzer, O. Haas, Electrochim. Acta 47 (2002) 3995.
[2] M.J. Montenegro, T. Lippert, S. Muller, A. Weidenkaff, P.R. Willmott, A. Wokaun, Appl. Surf. Sci. 197–198 (2002) 505.
[3] J. Ponce, J.-L. Rehspringer, G. Poillerat, J.L. Gautier, Electrochim. Acta 46 (2001) 3373.
[4] R.N. Singh, B. Lal, Int. J. Hydrogen Energy 27 (2002) 45–55.
[5] S.K. Tiwari, S.P. Singh, R.N. Singh, J. Electrochem. Soc. 143 (1996) 1493.
[6] A.N. Jain, S.K. Tiwari, P. Chartier, R.N. Singh, J. Chem. Soc., Faraday Trans. 91 (1995) 187.
[7] N.-L. Wu, W.-R. Liu, S.-J. Su, Electrochimica Acta 48 (2002) 1567.
[8] O. Haas, F. Holzer, S. Muller, J.M. McBreen, et al., Electrochim. Acta 47 (2002) 3211.
[9] H. Arai, S. Müller, O. Haas, J. Electrochem. Soc. 147 (2000) 3587.
[10] E. Yeager, Electrochim. Acta 29 (1984) 1527.
[11] R.N. Singh, B. Lal, Int. J. Hydrogen Energy 27 (2002) 44.
[12] G. Xiong, Z. Zheng-Liong, X. Yang, L. Lude, X.J. Wang, Mater. Sci. Lett. 16 (1997) 1064.
[13] R. Othman, W.J. Basirun, A.H. Yahaya, A.K. Arof, J. Power Sources 103 (2001) 34.
[14] E. Rios, J.-L. Gautier, G. Poillerat, P. Chartier, Electrochim. Acta 44 (1998) 1491.
[15] J. Prakash, D.A. Tryk, E.B. Yeagerc, J. Electrochem. Soc. 146 (1999) 4145.
[16] Z. Wei, W. Huang, S. Zhang, J. Tan, J. Power Sources 91 (2000) 83.